Flow-forced dynamics of a triple heat exchanger—Part II: Experimentation and results

P. C. Chiu
Department of Mechanical Engineering, University of Hong Kong, Hong Kong

E. H. K. Fung
Department of Mechanical and Marine Engineering, Hong Kong Polytechnic, Hong Kong

Fluid temperature transients in an experimental triple heat exchanger system were obtained for step-like changes of the primary loop, carrier loop and secondary shell fluid flow-rates. Numerical results obtained from the proposed dynamic model were shown to be in general agreement with the experimental responses.

Keywords: heat exchangers; dynamic model; weighted residuals

Introduction

Flow-forced dynamics of a triple heat exchanger system has practical importance in that it simulates, for example, the system behavior of a nuclear power plant under turbine load disturbance condition. Under such circumstances, the control system must first manipulate the steam and intermediate fluid flow-rates, since the heat source is usually remotely placed from the turbine and a large amount of energy is stored in the plant. In the case of load increase, the steam flow-rate is raised. The energy stored in the plant is temporarily reduced before it is eventually restored by the increase of heat input to the plant. Similar examples occur in the solar heating and solar air-conditioning systems.

Experimental study of the temperature transients of a double-pipe heat exchanger subjected to the flow disturbances has been most recently studied by Gilles.[1] He derived a linearized model represented by a transcendental transfer matrix and concluded that his model, including the variation of heat transfer coefficient with both the flow-rate and temperature and the wall dynamics, agreed closely with the experimental results. Temperature transients of an interconnected heat exchanger were first studied by Thal-Larsen and Loscutoff.[2] They built a dual heat exchanger in which one circulation loop was formed by linking two double-pipe heat exchangers. Experiments showed that, due to the presence of positive feedback, an oscillatory transient occurred in the discharge temperature for a step-like change in flow-rate of the circulating fluid. After failing to obtain a satisfactory lumped simulation model for the dual heat exchangers, they proposed an empirical analogue model with the parameters chosen to match the experimental transients.

An experimental triple heat exchanger was designed and built in order to verify the dynamic results obtained from the derived model. Design consideration was focused on an attempt to obtain a simple but accurate model of the pilot plant and on exposing the basic characteristics of the triple heat exchanger subjected to various types of disturbances. From the process control point of view, a triple heat exchanger is a multivariable, nonlinear and distributed parameter system. Before the flow-forced dynamics of the triple heat exchanger could be studied, it is necessary to fully comprehend the flow-forced dynamics of the individual heat exchangers and also to recognize that positive feedbacks are present because of the two circulating loops. Temperature oscillations are therefore likely to occur for a change of the primary loop fluid flow-rate or the carrier loop fluid flow-rate.

Address reprint requests to Dr. Chiu at the Department of Mechanical Engineering, University of Hong Kong, Hong Kong.

Received 7 June 1988; accepted 8 June 1989

The triple heat exchanger

The general layout of the experimental triple heat exchanger is shown in Figure 1. It consists of one STHE and two DPHE connected by four connecting pipes to form two circulating loops. Each externally insulated DPHE was constructed by mounting a 25.0mm i.d. and 27.8mm o.d. hard brass tube concentrically in a 53.2mm i.d. and 58.8mm o.d. hard brass tube and supported at each end by a headstock. The STHE was built by installing six pairs of two-kilowatt and one-kilowatt coiled immersion heaters in an insulated brass tube of 76.2mm i.d. and 78.7mm o.d. The heaters were positioned so

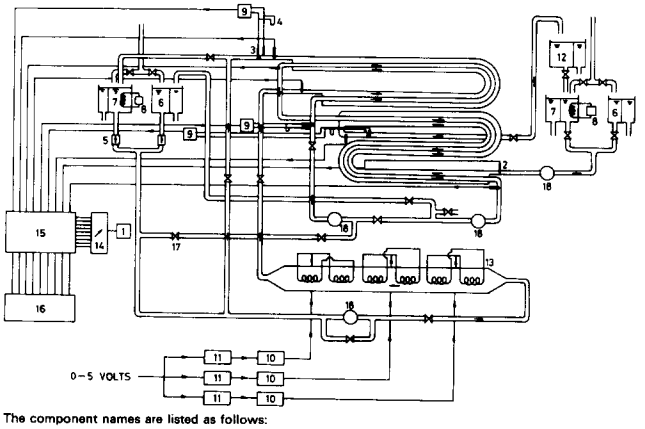

The component names are listed as follows:

1. Digital multimeter
2. Thermocouples (chrome-alumel)
3. Pitot and static tubes
4. Manometers
5. Non-return valves
6. Cold water tanks
7. Hot water tanks
8. Immersion heaters and temperature controller
9. Differential pressure transducers
10. Thyristor
11. Power controller
12. Feedback tank
13. Immersion heaters (single tube heat exchangers)
14. Thermocouple switch
15. Two-way switches
16. Oscillograph
17. Gate valves
18. Centrifugal pumps

Figure 1 Schematic plant layout of triple heat exchanger system

that the plane of the heating coils was perpendicular to the direction of flow to minimize the obstruction to the flow. The connecting pipes were made of mild steel with 23.4mm i.d. and 26.6mm o.d. Two diffusers were fitted at the ends of the STHE by means of flanges so as to connect up the steel pipes. The lengths of the heat exchangers and the connecting pipes are $L_1=7.87$m, $L_2=15.75$m, $L_5=3.56$m, $L_6=7.70$m, $L_7=1.19$m, $L_8=11.56$m, and $L_9=3.78$m. The two water streams in the primary heat exchanger were flowing in a parallel-flow condition while those in the secondary heat exchanger were flowing in a counter-flow condition. The outer surfaces of the heat exchangers and the pipes were insulated. The selection of suitable centrifugal pumps for primary and carrier loops was done by experimental trial until the size and combination of the pumps satisfied the flow requirement.

Changes of heating rate could be made by adjusting the voltage signals to the thyristor power controllers which controlled the power output of the immersion heaters. The inlet temperature of the secondary heat exchanger could be set at any value within the limits by mixing the cold water and hot water streams. The hot water was issuing from a tank inside which an Eurotherm temperature controller was installed. The cold water stream was issuing from a tank which could be supplied with fresh tap water, or water pumped from the sump or both, depending on the tap water temperature. Changes of each of the circulating water flow-rates or the shell water flow-rate of the secondary heat exchanger could be made by adjusting the setting of an appropriate gate-valve.

For steady-state and transient testings of the triple heat exchanger, chromel–alumel thermocouples of K type were used to measure the temperatures of water. Each thermocouple was calibrated against a standard mercury-in-glass thermometer with an accuracy of ± 0.02°C. The hot junctions of the thermocouples penetrated into the heat exchanger at eight different locations with the cold junctions immersed in a well stirred bath of melting ice. The temperature transients were recorded on a twelve-channel ultraviolet oscillograph by connecting each thermocouple output to a sensitive galvanometer. Pitot and static tubes were used to measure the water flow-rates by calibrating the dynamic head at the central position of the pipe flow against the measured flow-rates. In order to record the velocity change during the transient testing, three differential pressure transducers Type No. PTD 310-D manufactured by Schaevitz Engineering were employed to convert the differential pressure signals from the pitot and static tubes to electric signals of ± 2.5V. The transducer signals were also recorded in the ultraviolet oscillograph recorder.

Computation of heat transfer coefficients

The overall heat transfer coefficients of the two DPHE and the heat loss coefficients were computed by substituting the experimental data to the steady-state temperature equations. For the primary heat exchanger, the steady-state temperature equations may be obtained from Equations 1 and 2 of the Part I of this paper by putting the temperature–time derivative terms to zero and the solutions are expressed as follows

$$T_p(L_1)=e^{-g_4L_1}(\cosh g_5L_1-g_6\sinh g_5L_1)T_p(0)+g_7e^{-g_4L_1}(\sinh g_5L_1)T_{c1}(0)+(1-e^{-g_4L_1}\cosh g_5L_1-g_8e^{-g_4L_1}\sinh g_5L_1)T_a \quad (1)$$

$$T_{c1}(L_1)=e^{-g_4L_1}(\cosh g_5L_1+g_6\sinh g_5L_1)T_{c1}(0)-g_9e^{-g_4L_1}(\sinh g_5L_1)T_p(0)+(1-e^{-g_4L_1}\cosh g_5L_1-g_{10}e^{-g_4L_1}\sinh g_5L_1)T_a \quad (2)$$

where

$$g_1=\frac{2\pi r_{m,1}U_1}{\dot m_{1,1}c_{1,1}} \qquad g_2=\frac{2\pi r_{4,1}h_{L,1}}{\dot m_{1,1}c_{1,1}}$$

$$g_3=-\frac{2\pi r_{m,1}U_1}{\dot m_{2,1}c_{2,1}} \qquad g_4=\frac{g_1+g_2-g_3}{2}$$

$$g_5=[g_2g_3+g_4^2]^{\frac{1}{2}} \qquad g_6=\frac{g_1+g_2+g_3}{2g_5}$$

$$g_7=\frac{g_1}{g_5} \qquad g_8=\frac{g_1-g_2-g_3}{2g_5}$$

$$g_9=\frac{g_3}{g_5} \qquad g_{10}=\frac{g_4}{g_5}$$

The values of U_1 and $h_{L,1}$ were determined from the simultaneous implicit Equations 1 and 2 by substituting experimental data $T_p(0)$, $T_{c1}(0)$, $T_p(L_1)$, $T_{c1}(L_1)$, and T_a. It was found that $h_{L,1}=0.687\times10^{-2}$ kW m^{-1} K^{-1}. Similarly, the steady-state temperature equations of the secondary heat exchanger may be obtained from Equations 3 and 4 of the Part I of this paper as follows

$$T_s(L_2)=e^{-g_{14}L_2}(\cosh g_{15}L_2-g_{16}\sinh g_{15}L_2)T_s(0)+g_{17}e^{-g_{14}L_2}(\sinh g_{15}L_2)T_{c2}(0)+(1-e^{-g_{14}L_2}\cosh g_{15}L_2-e^{-g_{14}L_1}g_{18}\sinh g_{15}L_2)T_a \quad (3)$$

$$T_{c2}(L_2)=e^{-g_{14}L_2}(\cosh g_{15}L_2+g_{16}\sinh g_{15}L_2)T_{c2}(0)-g_{19}e^{-g_{14}L_2}(\sinh g_{15}L_2)T_s(0)+(1-e^{-g_{14}L_2}\cosh g_{15}L_2-g_{20}e^{-g_{14}L_2}\sinh g_{15}L_2)T_a \quad (4)$$

where

$$g_{11}=-\frac{2\pi r_{m,2}U_2}{\dot m_{1,2}c_{1,2}} \qquad g_{12}=-\frac{2\pi r_{4,2}h_{L,2}}{\dot m_{1,2}c_{1,2}}$$

$$g_{13}=-\frac{2\pi r_{m,2}U_2}{\dot m_{2,2}c_{2,2}} \qquad g_{14}=\frac{g_{11}+g_{12}-g_{13}}{2}$$

$$g_{15}=[g_{12}g_{13}+g_{14}^2]^{\frac{1}{2}} \qquad g_{16}=\frac{g_{11}+g_{12}+g_{13}}{2g_{15}}$$

$$g_{17}=\frac{g_{11}}{g_{15}} \qquad g_{18}=\frac{g_{11}-g_{12}-g_{13}}{2g_{15}}$$

$$g_{19}=\frac{g_{13}}{g_{15}} \qquad g_{20}=\frac{g_{14}}{g_{15}}$$

The value of h_{L2} was found to be zero. This was expected since the secondary heat exchanger was operated at lower temperatures.

For the STHE, the constants for the k_1 and k_2 for the heat loss term is obtained from

$$qL_5=\dot m_5c_5[T_5(0,L_5)-T_5(0,0)]+\int_0^{L_5}k_2\left\{T_5(0,0)+\left[\frac{T_5(0,L_5)-T_5(0,0)}{L_5}\right]x-T_a\right\}^{k_1}dx \quad (5)$$

where q is the electrical power input. The constants k_1 and k_2 were evaluated for different values of q, T_a, $T_5(0,0)$, $T_5(0,L_5)$, and $\dot m_5$. The values of k_1 and k_2 were found to be 3.15 and 5.97×10^{-6}. Because of the construction of the heater, it was not insulated at its ends so that the wire would not be overheated. Therefore the heat loss of the STHE was mainly contributed by the exposed ends of the heaters as well as by

the wall. The value of k_1 clearly indicated that the heat transfer to the surroundings was partly through radiation process from the uncovered parts of the heaters. In general, it was found that the heat loss of the primary heat exchanger was about 1 to 2%, and that of the STHE was about 4 to 5%.

Validation of assumptions

The assumptions as stated in Part I of this paper need to be validated for the present configuration of the heat exchangers. With the exception of the viscosity, the three general assumptions are commonly accepted in most of the heat exchanger analysis. Gilles[1] proposed that the heat transfer coefficients in a DPHE varied with respect to the flow-rate as well as the temperature since the viscosity of the water is temperature dependent and the heat transfer coefficients may be calculated from the Dittus–Boelter formula. However as the temperature variation of the present experiments never exceeded 8°C, the assumption that the heat transfer coefficients are independent of temperature and viscosity is valid. The heat transfer coefficient in a DPHE is therefore only dependent on the velocity as stated in assumption 6 (Part I).

The most important assumption for the DPHE is that the tube wall and shell wall thermal capacitances are additive to those of the tube liquid and shell liquid respectively. If the dynamics of the tube wall and shell wall are considered, four partial differential equations are necessary. With this assumption, only two partial differential equations are necessary for the model. The former is named Model A and the latter is named Model B. For the present configuration, thin wall brass tubes were purposely chosen and the ratios of the thermal capacitances of the walls to those of liquids are given as follows: $f_{1,1}=0.1503$, $f_{2,1}=0.1868$, $f_{1,2}=0.1505$, and $f_{2,2}=0.1468$. An earlier study[3] had shown that both models agreed closely with the experimental results. However, Model A gave a slightly more accurate response and Model B tended to give slightly slower initial response but faster settling time. Model B was preferred to Model A for the following reasons: (a) when applied to Model B, the MWR formulation yielded a comparatively stable solution; (b) less computation time was needed for the two-equation model since the system equation was of lower dimension. The increase in computer time was not justified for a slight improvement in accuracy. For the same reasons, as both the STHE and the connecting pipes were chosen to have thin metal walls, the assumptions 9 and 12 were made (see Part I). The values of f_5 and f were 0.1247 and 0.2294 respectively.

Assumption 6 (Part I) was found to be closely in agreement with the experiment. The values of constants p_1 and p_2 for each DPHE were determined by least square fit of sixteen values of U calculated from Equations 1–4 for different flow-rates. They were $p_{1,1}=6.70$, $p_{2,1}=3.50$, $p_{1,2}=5.37$, and $p_{2,2}=4.51$. Since the values of U and h_L for computer simulation were calculated from the values of p's obtained from the above general fit, small deviations of initial steady-state temperatures at inlet and outlet of individual heat exchangers from the experimental data were expected. The computed initial steady-state temperature could be made equal to the experimental data, if the values of U and h_L were computed from a specific set of initial and final steady-state experimental data. In this case assumption 6 would not apply, and the generality of the model prediction would be lost.

Assumption 7 (Part I) by linearizing the change of U with respect to the change of flow-rate was made to simplify formulation of the mathematical model and to minimize the computer time. In comparison with the estimated U from the above procedure, the linearization tended to underestimate U by a maximum of about 5% for the range of change in flow-rate. However since the response of the step-like change in flow-rate is much faster than those of temperature responses, the error incurred is negligible.

Assumption 13 (Part I), that the heat loss of connecting pipes was negligible, was made in accordance with the experimental data. The temperature drop in the two connecting pipes between the STHE and the primary heat exchanger was about 0.1°C and was lumped to the heat loss of the STHE. No temperature drop in the other two connecting pipes were observed. Further heat balance showed that, for the secondary heat exchanger, the heat loss to the surroundings was also negligible. These were expected because the pipes and the secondary heat exchanger were operated at lower temperatures.

There was an additional assumption which has not been stated in the Part I of the paper. The mass of the liquid contained in each of the two diffusers and its metal mass were approximated to the equivalent length of the connecting pipe by volume balance. The values of L_8 and L_9 had taken into account the equivalent lengths of the diffusers.

Results and discussion

The governing matrix differential equation, Equation 33 is solved numerically in the VAX 11/780 digital computer using the fourth order Runge–Kutta method to yield the temperature transients for a step-like change of flow-rate. Experimental results were obtained for both upstep and downstep flow disturbances under two sets of heat rate and flow conditions. Comparison shows that the two sets of results have similar trend. Only the set with high heating and high flow is presented together with the computed responses. In Figures 2–6, the experimental results are represented by lines and the computed results by points. The steady-state temperature data for upstep and downstep changes of flow disturbances are presented in Tables 1a and 1b respectively. The computed initial steady-state temperatures were obtained by substituting the heat transfer and heat loss coefficients of the general fit to Equations 1–5. The computed final steady-state temperatures were obtained by superimposing the steady-state temperature changes computed from Equation 33 of the Part I of the paper to the initial data. Both Tables 1a and 1b show that deviations between computed and experimental temperature data exist, which are attributed to the fact that the constants k_1, k_2, p_1, and p_2 were derived by the general fits of experimental data.

Physically, the damped oscillations of the temperature responses produced by step-like disturbances in the primary flow and carrier flow as shown in Figures 2–5 are attributed to two main considerations. Firstly, the oscillations are due wholly to the temperature changes caused by the heat imbalance as the result of the change in flow and the positive feedback characteristics. Secondly, a DPHE exhibits inherent damping characteristic, due to (1) increase in temperature difference between the two fluids tending to increase heat transfer rate that will reduce that difference, and (2) the increase of heat transfer rate as the result of increase of flow-rate. On the other hand, the heat transfer rate in the STHE is not affected by the fluid temperature in it nor by the fluid velocity. The STHE therefore tends to offer very little damping effect to the system. It can be deduced that the primary loop offers much less damping effect than that of the carrier loop, and therefore plays a dominant role on temperature oscillation characteristics in the system. In the following discussion, reference must be made to the schematic diagram of the triple heat exchanger as shown in Figure 1 of the Part I of the paper.

The temperature responses for a step-like increase of primary

Table 1 Steady-state data for various flow disturbances; I = initial state, F = final state, ( ) = computed value, other data obtained from experiment

(a) up step flow changes

Disturbance type		q (KW/m)	$\dot{m}_{1,1}$ (kg/s)	$\dot{m}_{2,1}$ (kg/s)	$\dot{m}_{1,2}$ (kg/s)	$T_p(0)$ (°C)	$T_p(L_1)$ (°C)	$T_{c1}(0)$ (°C)	$T_{c1}(L_1)$ (°C)	$T_s(0)$ (°C)	$T_s(L_2)$ (°C)	T_e (°C)
Primary loop fluid flow-rate change	I	5.36	0.31	0.39	0.47	72.9 (74.1)	60.2 (61.2)	39.4 (39.6)	49.2 (49.6)	39.1 (39.2)	30.9	28.5
	F	5.36	0.49	0.39	0.47	68.2 (69.3)	59.9 (60.6)	39.7 (39.8)	49.9 (50.1)	39.4 (39.4)	30.9	28.5
Carrier loop fluid flow-rate change	I	5.19	0.49	0.22	0.47	74.0 (72.9)	66.0 (65.2)	38.2 (37.9)	55.4 (54.4)	39.5 (39.1)	31.3	27.5
	F	5.19	0.49	0.36	0.47	69.2 (68.3)	60.9 (60.2)	40.1 (39.9)	51.1 (50.4)	39.8 (39.6)	31.3	27.5
Secondary fluid flow-rate change	I	5.46	0.49	0.39	0.31	74.1 (74.3)	66.2 (66.4)	47.2 (47.1)	56.9 (56.8)	47.1 (47.0)	34.7	26.5
	F	5.46	0.49	0.39	0.47	71.4 (71.6)	63.2 (63.3)	43.3 (43.2)	53.4 (53.3)	43.1 (43.0)	34.7	26.5

(b) down step flow changes

Disturbance type		q (KW/m)	$\dot{m}_{1,1}$ (kg/s)	$\dot{m}_{2,1}$ (kg/s)	$\dot{m}_{1,2}$ (kg/s)	$T_p(0)$ (°C)	$T_p(L_1)$ (°C)	$T_{c1}(0)$ (°C)	$T_{c1}(L_1)$ (°C)	$T_s(0)$ (°C)	$T_s(L_2)$ (°C)	T_e (°C)
Primary loop fluid flow-rate change	I	5.36	0.49	0.39	0.47	68.2 (69.1)	59.9 (60.6)	39.7 (39.8)	49.9 (50.1)	39.4 (39.5)	30.9	28.5
	F	5.36	0.31	0.39	0.47	72.9 (74.0)	60.2 (61.2)	39.4 (39.6)	49.2 (49.6)	39.1 (39.3)	30.9	28.5
Carrier loop fluid flow-rate change	I	5.19	0.49	0.36	0.47	69.2 (68.5)	60.9 (60.4)	40.1 (39.8)	51.1 (50.5)	39.8 (39.5)	31.3	27.5
	F	5.19	0.49	0.22	0.47	74.0 (73.4)	66.0 (65.6)	38.2 (37.9)	55.4 (54.7)	39.5 (39.1)	31.3	27.5
Secondary fluid flow-rate change	I	5.46	0.49	0.39	0.47	71.4 (71.5)	63.2 (63.3)	43.3 (43.2)	53.4 (53.3)	43.1 (43.0)	34.7	26.5
	F	5.46	0.49	0.39	0.31	74.1 (74.3)	66.2 (66.5)	47.2 (47.2)	56.9 (56.9)	47.1 (47.0)	34.7	26.5

flow-rate are shown in Figure 2. Consider the response of $T_p(t, 0)$, which decreases because of decrease of heat transfer per unit mass of primary fluid at the outlet of the STHE. Therefore cold slug is produced at $T_p(t, 0)$. In the primary heat exchanger, the carrier fluid temperature $T_{c1}(t, L_1)$ tends to increase due to increase of heat transfer coefficient caused by the increase in primary flow-rate. On the other hand, the change of temperature of the primary fluid $T_p(t, L_1)$ is less predictable. Two conflicting effects are working, firstly the increase of primary flow decreases the heat transfer rate from a unit mass of primary fluid tending to increase the primary fluid temperature, and secondly increase in heat transfer coefficient increases the heat transfer rate from a unit mass of primary fluid tending to decrease the primary fluid temperature. The net effect can be confirmed by calculation from the steady-state data. It can be easily seen from the response of $T_p(t, L_1)$ that the first effect plays the dominant role on the transient response while the second effect mainly influences the steady-state temperature. In the primary loop, therefore, a cold slug is formed at the outlet of the STHE while a hot slug is produced at the outlet of the primary heat exchanger. The circulation of the hot and cold slugs produces temperature oscillations in the primary loop. However, oscillations in $T_p(t, 0)$ and $T_p(t, L_1)$ are eventually damped down by the inherent damping characteristics of a heat exchanger.

As explained earlier, the carrier fluid temperature at the outlet of the primary heat exchanger $T_{c1}(t, L_1)$ increases for an increase in primary flow-rate. A hot slug is thus formed at $T_{c1}(t, L_1)$. The cold slug originated at the STHE outlet will act as a disturbance on reaching the primary heat exchanger, which subsequently causes a decrease in $T_{c1}(t, L_1)$, producing a cold slug. These hot and cold slugs in the carrier loop, which are induced by the temperature oscillations in the primary loop, are heavily attenuated in magnitude as they pass through the secondary heat exchanger which has the damping effect as mentioned before. Thus the temperature oscillations of the fluid in the carrier loop $T_{c1}(t, L_1)$ and $T_{c2}(t, L_2)$ are first created and then dominated by the oscillations in the primary loop. The temperature oscillations in the carrier loop that are fed through the primary heat exchanger are thus relatively small in magnitude compared to those in the primary loop.

The temperature responses for a step-like decrease of primary flow-rate are shown in Figure 3. In general they show similar trend. The oscillatory temperature response may be described by (1) the time to reach the maximum excursion; (2) the magnitude of maximum excursion, (3) the period of oscillation; and (4) the decay rate. (2) and (4) are related to the overall system parameters and are difficult to make a simple explanation or calculation. One will deduce that the period of temperature oscillation is directly related to the circulation time of the primary loop, which is equal to the sum of distances over the corresponding velocities in the loop. Measurements made on the response curves for the two sets of flow conditions and partly shown in Table 2 indicate that the deduction is correct and the period of oscillation of the temperature responses in the two loops for a primary flow-rate change is not influenced

by the circulating time of the carrier loop.

The temperature responses due to a step-like increase of carrier flow-rate produce similar oscillations as shown in Figure 4. In this case, a cold slug $T_{c1}(t, L_1)$ is formed at the outlet of the primary heat exchanger, while a hot slug $T_{c2}(t, L_2)$ is formed at the outlet of the secondary heat exchanger. Circulation in the carrier loop of the hot and cold slugs again produces temperature oscillations. In the same way, the hot and cold slugs are also induced in the primary loop due to the temperature oscillations of the carrier loops. As expected, the oscillatory responses for a disturbance of carrier flow-rate produce heavier damping than those obtained from that of primary flow. This is also confirmed by the temperature responses due to a step-like decrease of carrier flow-rate as shown in Figure 5. Measurements on the response curves as shown in Table 2 reveal that the periods of oscillations for all temperatures are primarily related to the circulation time of the primary loop but are also influenced by the circulation time of the carrier loop. Comparison of the computed and experimental responses show that the experimental period of oscillation is in general very close to its computed value.

Figure 6 indicates that for secondary flow disturbance the temperature responses show no oscillation. This may be explained by the fact that heavy damping effect is present in the carrier loop and the secondary heat exchanger.

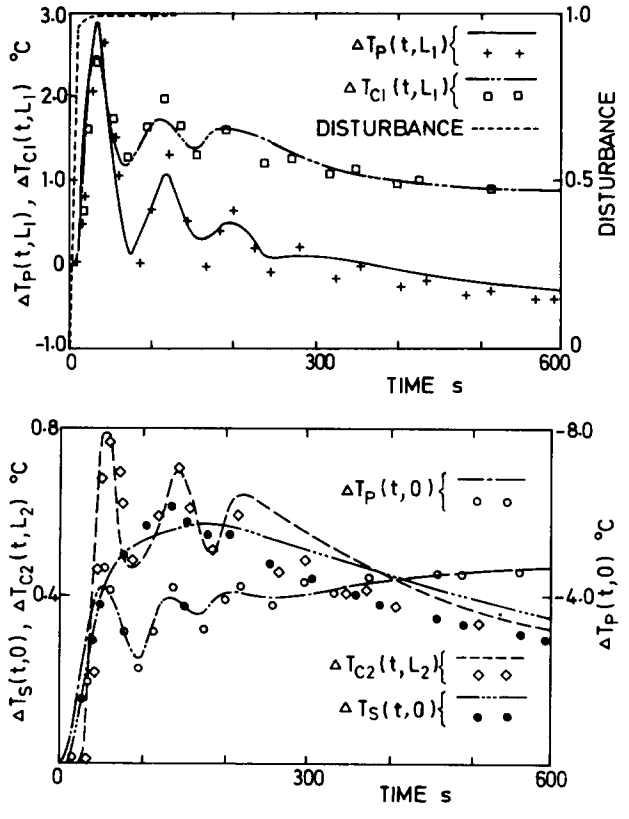

Figure 2 [(a) and (b)]. Temperature transients for an increase in primary flow-rate $\dot{m}_{1,1}$ (0.31 kg/s to 0.49 kg/s), $q = 5.36$ kw/m, $\dot{m}_{2,1} = 0.39$ kg/s, $\dot{m}_{1,2} = 0.47$ kg/s

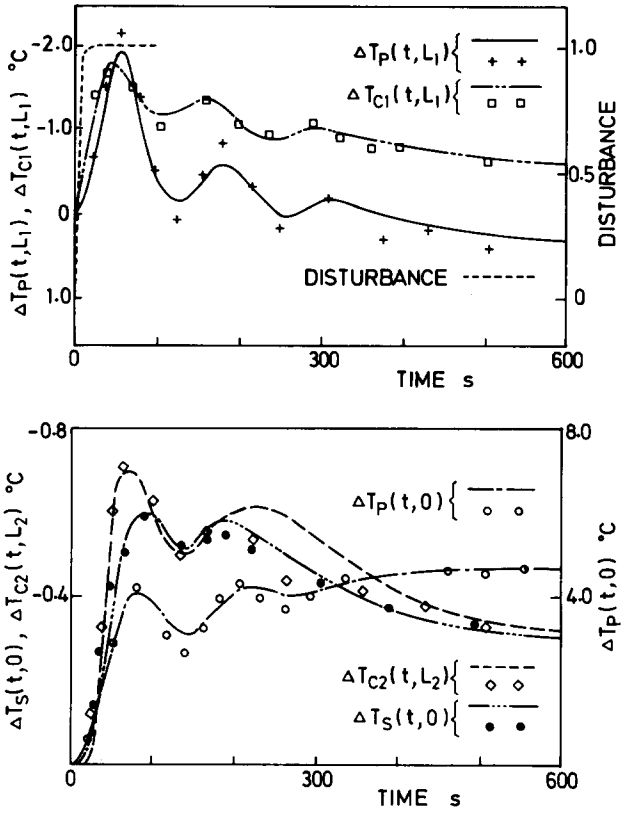

Figure 3 [(a) and (b)]. Temperature transients for a decrease in primary flow-rate $\dot{m}_{1,1}$ (0.49 kg/s to 0.31 kg/s), $q = 5.36$ kw/m, $\dot{m}_{2,1} = 0.39$ kg/s, $\dot{m}_{1,2} = 0.47$ kg/s

Table 2 Period of transient oscillations (s) and circulation times (s) for flow disturbances

Temperature response	Primary flow disturbance				Carrier flow disturbance			
	Increasing		Decreasing		Increasing		Decreasing	
	τ_p	τ'_p	τ_p	τ'_p	τ_p	τ'_p	τ_p	τ'_p
$T_p(t, 0)$	83.1	81.8	147.1	125.3	74.1	73.0	93.4	82.5
$T_p(t, L_1)$	85.7	81.1	128.9	125.3	69.6	68.0	97.5	82.5
$T_{c1}(t, L_1)$	81.8	81.1	121.5	120.2	86	76.5	92.6	82.5
$T_{c2}(t, L_2)$	87.0	86.0	153.5	122.8	61.1	58.4	77.0	68.8
τ_{cp}	69.4		109.1		69.4		69.4	
τ_{cc}	40.5		40.5		43.6		71.2	

τ_{cc}, τ_{cp} = circulation time of carrier and primary loops respectively
τ_p, τ'_p = period of oscillation of experimental and computed responses respectively

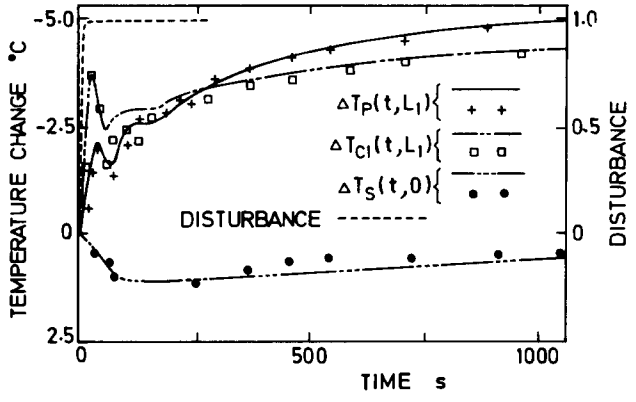

Figure 4 Temperature transients for an increase in carrier flow-rate $\dot{m}_{2,1}$ (0.22 kg/s to 0.36 kg/s), $q=5.19$ kw/m, $\dot{m}_{1,1}=0.49$ kg/s, $\dot{m}_{1,2}=0.47$ kg/s

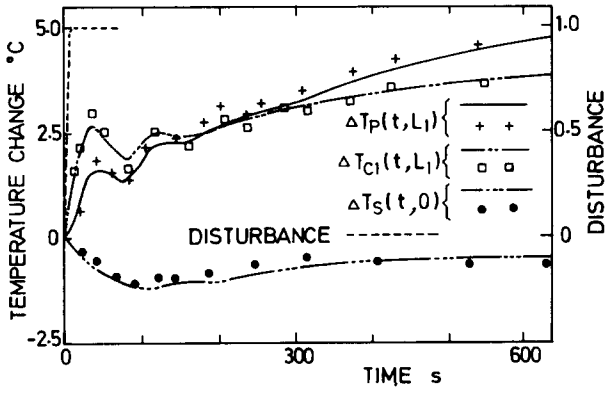

Figure 5 Temperature transients for a decrease in carrier flow-rate $\dot{m}_{2,1}$ (0.36 kg/s to 0.22 kg/s), $q=5.19$ kw/m, $\dot{m}_{1,1}=0.49$ kg/s, $\dot{m}_{1,2}=0.47$ kg/s

The study shows that MWR method of evaluating transient responses using the governing partial differential equations predicts the experimental responses with acceptable accuracy. In the process of computation, the largest integration time step to ensure stable solution was found to be less than one quarter to half of the smallest delay time. The initial spurious oscillations with small amplitude were experienced when evaluating the transient responses with large pure time delay. Further, the computed responses are in general more oscillatory than the experimental ones.

It should be noted that the present work only exposes the flow-forced temperature dynamics of the particular experimental triple heat exchanger under testing, where the phase change and other complex thermodynamic and heat transfer behavior have not taken place as in the nuclear power plant. The oscillatory behavior of the temperature response has been magnified by the particular geometry and configuration of the heat exchangers chosen, as the dimensions of the heat exchanger are of the similar order and pure time delay plays significant role in the dynamic behavior. In most practical applications,

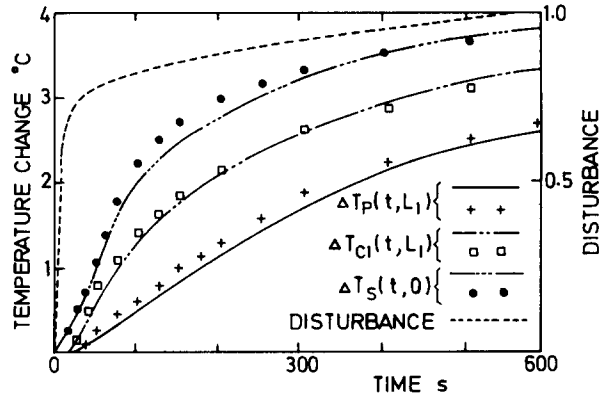

Figure 6 Temperature transients for a decrease in secondary flow-rate $\dot{m}_{1,2}$ (0.47 kg/s to 0.31 kg/s), $q=5.46$ kw/m, $\dot{m}_{1,1}=0.49$ kg/s, $\dot{m}_{2,1}=0.39$ kg/s

such temperature oscillation must be eliminated or significantly damped. Preliminary considerations indicate that the temperature oscillation may be damped by increasing the heat transfer coefficient, or increasing fluid mixing. However, further study is needed to gain a thorough physical understanding of the effect of these factors.

Conclusions

The weighted residual method of evaluating transient temperature responses from the governing partial differential equations predicts the experimental responses with good accuracy. For step-like changes of the primary and carrier flow-rates, temperature responses show damped oscillations which are attributed wholly to the creation of cold and hot slugs in the loops and the positive feedback characteristics. The temperature oscillations are predominant in the primary loop. They exhibit more lightly damped responses than those of the carrier loop. The periods of oscillation of temperature responses for a change of primary flow-rate are found to be primarily related to the circulation time of the primary loop. As for the carrier flow-rate change, the period of oscillation of all temperatures depends on the circulation times of both primary and carrier loops.

Acknowledgments

The work was supported by the University of Hong Kong Research Grants.

References

1 Gilles, G. New results in modeling heat exchanger dynamics. *Trans. ASME, J. Dynamic Systems, Measurement and Control*, 1974, **9**(3), 272–282

2 Thal-Larsen, H. and Loscutoff, W. V. Fluid-temperature transients in a dual-heat-exchanger system. *Trans. ASME, J. Basic Engng.*, 1964, **85**(1), 23–31

3 Chiu, P. C. and Fung, E. H. K. Temperature transients in a triple heat exchanger. *Proc. I. Mech. E.*, 1984, **198C**(12), 145–154